Silicon (2023) 15:1621–1633
https://doi.org/10.1007/s12633-022-02108-5

ORIGINAL PAPER

Investigating the Effect of Multi-pass Friction Stir Processing of SiC Particles on Temperature Distribution, Microstructure and Mechanical Properties of AA6061-T6 Plate

Setu Suman[1] · Durjyodhan Sethi[2] · Manish Bhargava[1] · Barnik Saha Roy[1]

Received: 1 July 2022 / Accepted: 7 September 2022 / Published online: 23 September 2022
© The Author(s), under exclusive licence to Springer Nature B.V. 2022

Abstract
In this paper, silicon carbide (SiC) particles were successfully inserted into AA6061-T6 aluminium matrix using multi-pass friction stir processing (MPFSP). The effects of MPFSP and SiC particles on temperature distribution, microstructural evolution, and mechanical properties are being investigated in detail. Processing was carried out at a constant process parameter, i.e., tool rotational speed of 1100 rpm, tool traverse speed of 1.5 mm/sec, and tool tilt angle of 2° to modify the microstructure and mechanical properties of MPFSP. It has been observed that SiC particles are not homogeneously distributed after the first pass, and particles congregate in some places. On the other hand, fourth-pass FSP results in a uniform distribution of particles. Agglomeration of SiC particles decreases with an increase in the number of passes and is uniformly distributed in the fourth pass of FSP. It has been observed that peak temperature, particle size, grain size, and mechanical properties are all influenced by MPFSP. The microhardness has significantly improved with increasing the number of passes. After MPFSP, the peak temperatures of the first pass, second pass, third pass, and fourth pass were recorded as 339.67 °C, 330.64 °C, 320.20 °C, and 312.81 °C, respectively, on the advancing side (AS), and similarly, on the retreating side (RS), 334.03 °C, 322.11 °C, 312.30 °C, and 303.72 °C, respectively. The values of the maximum ultimate tensile strength (UTS) and 0.2% yield stress were observed as 231 MPa, 247 MPa, 296 MPa, 308 MPa, and 178 MPa, 188 MPa, 202 MPa, and 225 MPa with the first pass, second pass, third pass, and fourth pass, respectively. But at the same time, % elongation decreased with an increase the number of passes.

Keywords Friction stir processing · Multi-pass · Reinforcement particle · SiC particle · Aluminium alloy

1 Introduction

Heat-treated AA6061-T6 is a precipitation hardened aluminium alloy attract the manufacturing and mineral processing industries due to their attributes i.e., excellent thermal conductivity, corrosion resistance, high strength-to-weight ratio, good castability and lower density, aluminium and its alloys are capable of meeting the demands [1–4]. These alloys are often utilised in the fabrication of missile casings, yacht construction, wings and fuselages and aviation landing mat [3–5].

FSP is a modified technique of friction stir welding process that was first devised and patented in 1991 by Wayne Thomas at The Welding Institute (TWI) [6]. Friction Stir processing, also known as surface modification technique, is the process of altering the microstructure and mechanical properties of base plates. Using nanoparticles in the processed zone, the parent metal's elongated and coarse grain structure were refined into the fine grain structure [7, 8]. FSP works on a similar approach to FSW, detailed explanations of the FSW process are available in the literature [6, 9, 10]. The FSP method has mostly been used to construct aluminium metal matrix composite (AMMCs) using nanoparticles [11, 12], with a few researchers studying multi-pass FSP for nanoparticle dispersion [13, 14]. A common FSP strategy is to change the mechanical characteristics and microstructure of metallic components. There are several methodologies for packing reinforcement

✉ Durjyodhan Sethi
durjyodhan84@gmail.com

[1] Department of Mechanical Engineering, National Institute of Technology, Agartala 799046, India

[2] Department of Mechanical Engineering, Gandhi Institute for Education and Technology, Baniatangi, Khurda 752060, India

particles, such as the groove technique [15, 16], holes method [17], direct pasting [18], and spray method [19]. Among these approaches, the groove methodology is considered to be the most efficacious [20, 21]. Various types of reinforcing particles including as SiC, TiC, B_4 C, Al_2O_3, Ti B_2, and others have been effectively integrated throughout aluminium alloy-based metal matrices via FSP [22–25]. Among of them, SiC is a prominent reinforcement particle because to its advantageous qualities such as outstanding thermal sock resistance, high thermal conductivity, low thermal expansion, excellent wear resistance, high strength, hardness, low density, and ease of availability [26–29]. Ma et al. [29] study the effect of multiple-pass friction stir processing on the microstructure and tensile properties of a cast aluminum–silicon alloy. They also observed that SiC ceramic particles were homogeneously distributed throughout the entire processed stir zone produced by multi-pass FSP. Sun et al. [30] exhibited homogenous particle dispersion in a copper plate incorporating nanoparticles during second pass friction stir welding. Dolatkhah et al. [31] explored multi-pass FSP to prevent particle agglomeration and found that, the reinforcement particles were distributed uniformly and the grain size was reduced. The movement of material flow around the tool, which necessitates an understanding of the temperature profile in the weldment. The temperature distribution analogy, together with the incorporation of SiCp in the plates, provides knowledge that might be used in multi-pass FSPed. Manoj Kumar et al. [32] investigate the temperature distribution and material flow in AA6061-T6 friction stir welding. They found that temperature decreased further from the mixing zones and that temperature distribution is asymmetric, which is an important aspect of the FSW process.

Rathee et al. [33] Investigated the effect of SiC particles size on microstructural and mechanical properties of AA5059/SiC surface composites during multi-pass FSP. They infer from multiple passes that there is a considerable improvement in mechanical attributes. Husain Mehdi et al. [34] reported that in the five pass FSP, Nano SiC particles were completely and uniformly distributed. As the number of FSP passes increases, the agglomeration of SiC particles decreases. Sun YF et al. [30] studied the impacts of SiC particles on the mechanical and microstructure characteristics of a copper joint's FSW. They find that homogeneous dispersion of SiC particles in the weld zone (WZ) resulted in an increase in microhardness and UTS after second passes.

The objective of this study, which served as a fundamental investigation, was to analyse the effects of MPFSP on the temperature distribution in the weld region, microstructural characteristics, and mechanical properties of AA6061-T6 plates that were 6 mm thick plate. Using a constant process parameter for this purpose.

2 Materials and Method

As a base metal (BM), AA6061-T6 (Tempered Condition) plates of (150 × 120 × 6 mm) were adopted for the study. Tables 1 and 2 shows the chemical compositional and mechanical properties of BM. As a reinforcement, Silicon carbide powder with an average particle size of 1–40 µm were used. A square shaped groove (3 mm side) was cut along the centre line of the base plate (As shown in the Fig. 1) to preplace SiC particles. After that, the prepared plates were cleaned with acetone, then SiC powder was packed and compressed into the grooves. Initially, a pinless tool H-13 with an 18 mm shoulder diameter was used for capping the top surface of the groove (refer Fig. 2a). After this, final FSP were performed on sophisticated FSW machine setup (refer Fig. 3) using a H-13 tool steel with concave shoulder of 18 mm diameter, and a taper threaded pin profile with Pin length of 5.8 mm (refer Fig. 2b). the number of FSP pass varies between one to four, while the process parameters i.e., tool traverse speed (TTS) of 1.5 mm/sec, tool rotational speed (TRS) of 1100 rpm and tool tilt angle (TTA) of 2° was kept constant throughout MPFSP.

For thermal profile investigation a K-type chromel-alumal thermocouples of 15 Gauge AWG were inserted on the both advancing and retreating side of the weld in vertical position at a depth of 3.5 mm and 14 mm distance from the weld centre-line to measure the temperature achieved during the processing. Thermal profiles were recorded using a data acquisition system which is coupled with plate. The location of the thermocouple, which has inserted into the plate shown in Fig. 3.

Welded samples were cut from the centre of each pass in a direction perpendicular to the processing method for macro and microstructural investigation. The resulting samples were polished using 150 grit emery papers sequentially up to 2000 grit emery papers, followed by velvet cloth polishing with colloidal silica. After that, the samples were etched

Table 2 Mechanical Properties of AA6061-T6

Ultimate Tensile Strength (MPa)	Yield Strength (MPa)	Elongation (%)
315	255	10.8

Table 1 Chemical compositional of AA6061-T6 alloys (wt.%)

Elements	Si	Fe	Cu	Mn	Mg	Cr	Zn	Ti	Al
AA6061-T6	0.60	0.40	0.25	0.10	1.00	0.09	0.03	0.07	Balance

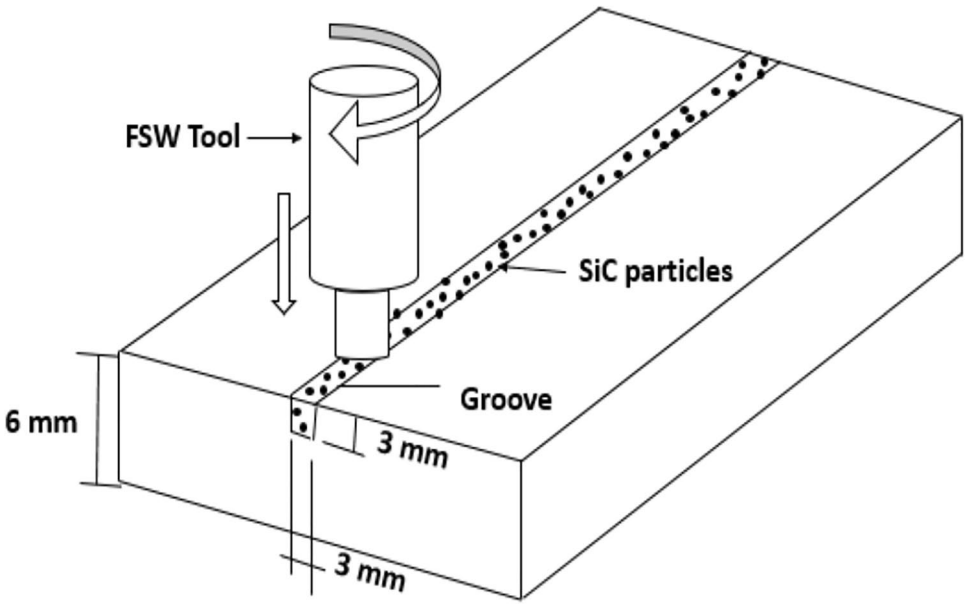

Fig. 1 Schematics diagram of base plate with groove

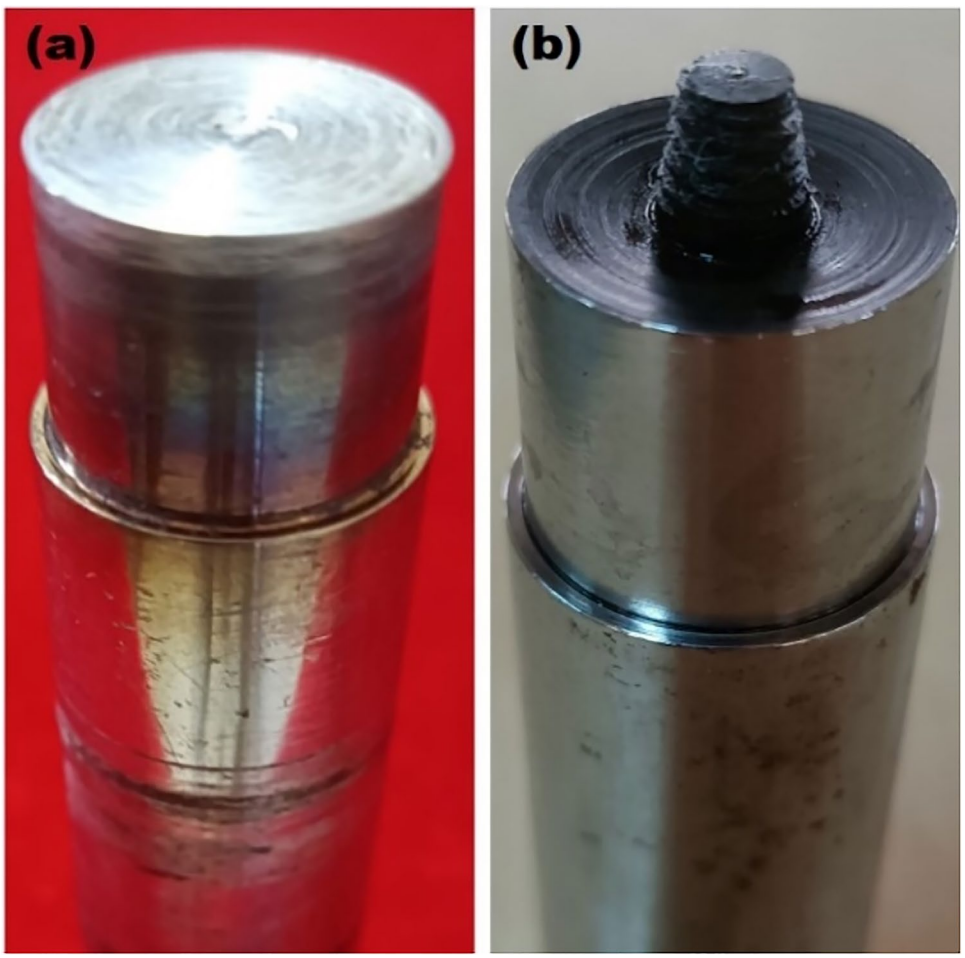

Fig. 2 FSP tool (**a**) Cover tool, (**b**) Welding tool

Fig. 3 Dedicated Friction stir welding setup

with Keller's reagent by dipping them for 10–15 s and then cleaned them with water or ethanol. The MPFSPed samples, microstructure and fractured surface was examined by Scanning Electron Microscope (SEM) and optical microscope. Vickers's microhardness tester was used to measure the microhardness of MPFSPed samples with a 100-gf load and a 10 s dwell period. In order to evaluate mechanical behaviour of MPFSPed, tensile specimens were cut perpendicular to the FSP direction.

3 Result and Discussion

3.1 The Effect of Multi-pass FSP AA6061-T6/SiCp on Temperature Distribution

It is well known that proper mixing of material by rotating tool shoulder and pin leads to an efficient FSW process which is directly dependent on temperature generated during the process [35]. Temperature is mainly generated due plastic deformation and frictional heat. Figure 4 shows the variation in the peak temperature profile varying FSP passes. All the thermal profiles were developed up to the time required to attain the room temperature after gradual cooling. Figure 4a reveals that maximum peak temperature 339.67 °C achieved during first pass FSP. The heat was transmitted to the base material during the processing after the first pass FSP material was preheated. Furthermore, increasing the number of FSP passes, the value of peak temperature of an individual thermocouple indicating decreases it may due to preheating of the material and other reason larger particles size, uneven distribution of particles. It has been observed that when the tool axis is close to the thermocouple point, the peak temperature is achieved in an instant for every process. From Fig. 4a, it can be observed that the peak temperature gradually decreases, as increases the number of FSP passes. Increasing the number of FSP passes leading to the breakdown the cluster of SiC particles resulting, grain refinement and strengthening the particles, reduces the particles agglomeration. According to [36] reported that addition of SiC powder in between two plates due to their higher thermal conductivity property we could achieve a higher peak temperature at higher tool rotational speed.

At fourth pass FSP, particles were homogeneously distributed, resulting minimum Peak temperature 312.81 °C was achieved. Observed from the Fig. 4c value of peak temperature was measured on the advancing side of the first, second, third, and fourth passes were 339.67 °C, 330.64 °C, 320.20 °C, and 312.81 °C, respectively, moderately higher than the retreating side was 334.03 °C, 322.11 °C, 312.30 °C, and 303.72 °C. similar studied by other researchers the peak temperature of the advancing side is significantly higher than the retreating side [37].

3.2 Crown Appearance of MPFSP AA6061-T6/SiCp

Figure 5a demonstrated the effect of reinforced SiCp with MPFSPed on AA6061-T6 plate. The FSP's crown looks to

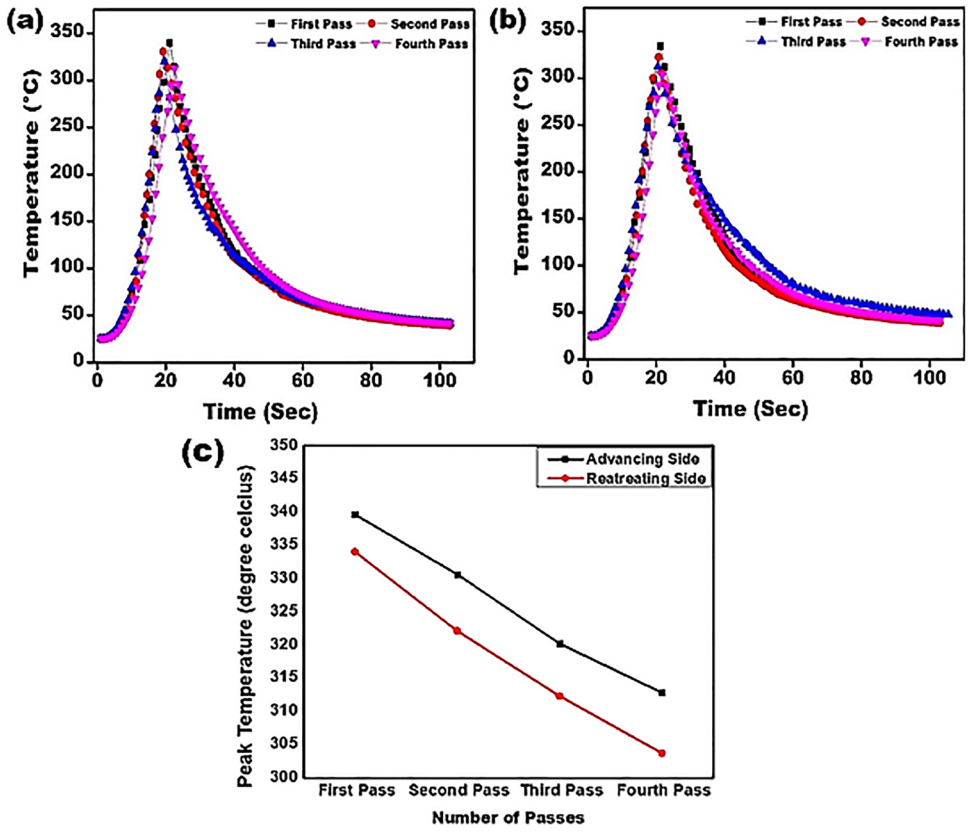

Fig. 4 Effect of MPFSP on Temperature profile at (**a**) advancing side, (**b**) retreating side and, (**c**) variation of peak temperature

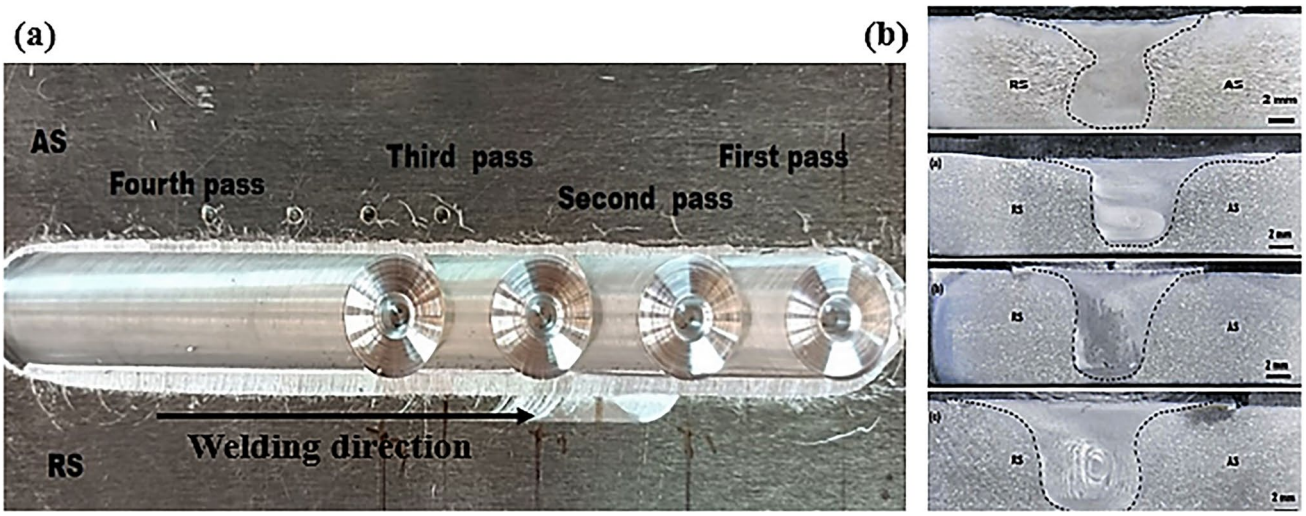

Fig. 5 (**a**) Weld surface appearance, (**b**) macrostructure of MPFSPed samples

be defect-free, as there are no flaws or irregularities present. Due to the rubbing action of the rotating tool shoulder on the workpiece, semi-circular geometries emerge as a crown. The soundness of the FSP zone is dictated by the crown's appearance. In all case, the macrostructure resembles symmetrical and elliptical in structure. The size and shape of stir zone (SZ) primarily depends on the processing parameters and tool geometry [38]. Figure 5b illustrates the macrostructure of MPFSP of AA6061-T6/SiC. On the photograph, the FSP zone's boundary is highlighted. On the processed plate, the common FSW imperfections such as warm holes, tunnels, and pin holes are not apparent. The macrostructure of the processed surface composite reveals a flattened and more uniform NZ width and nugget zone area. Also, it increases

the number of FSP passes, leading to an increase in the NZ area, as shown in Fig. 4b. At the constant chosen process parameters for all passes of FSP, the desired frictional heat generated is adequate for the uniform flow pattern of the plasticized material.

3.3 The Effect of Multi-pass FSP AA6061-T6/SiCp on Microstructure

A cross section of all processed samples was examined using an optical microscope and SEM for microstructural analysis to evaluate the distribution of reinforced particles and study the material flow characteristics. The microstructure of the NZ of different FSP pass with reinforcement particles is illustrated in Fig. 6. No internal defects were seen in all MPFSPed samples. Heat input strongly affected the microstructure of NZ, owing to intense plastic deformation and frictional heat, fine and equiaxed grain structure were found in the NZ as compared to other zones [39, 40]. As noticed from the Fig. 6a SiC particles were agglomerated in several regions, due to improper stirring tool action and lower FSP passes, perceived in first pass. According to [34] reported that, at the first pass, SiC powder with poor formability than the base material was concentrated inside the groove, so their flow was difficult, and most of them remained at the center of the NZ. However, with increasing the number of passes, found that less agglomeration and more uniform distribution of SiC particles. The refinement and uniformly distribution of the primary SiC nanoparticles were continuously improved as the FSP passes increased [41]. The grain size was decimated after the second pass FSP, leading to enhance material mixing and dispersion of reinforcement particles, as shown in Fig. 6b. It also observed that, the size of the reinforcement particles decreases continuously after each pass (to refer Fig. 6a-d).

The area fraction of the SiC reinforcement increased as the number of FSP passes increased, indicating a direct relation between FSP passes and particle distribution due to SiC particle fragmentation reduction [27]. According to Chang et al. [42] the fine and homogenous microstructure was found during MPFSP as a result of decreased heat input and strain build up owing to lower rotating speed.

Figure 6d shows that the grain size of SiC particles was decreased dramatically and homogeneously scattered in the fourth pass FSP compared to other passes. As the number of pass increases, the cluster of SiC particles begins to break down and uniformly distributed.

Figure 7a-d depicts the SEM image of the dispersion of SiC particles in NZ after the first, second, third, and fourth pass of FSP. The dispersion of particles is governed by the material flow in the NZ. The SEM micrograph of the NZ of first pass of FSP (Fig. 7a) reveals the uneven distribution of particles. The distribution of SiC particles was found to uniformly on increasing the number of passes from first to second, but slightly distribution of particles was observed in Fig. 7b. fragmentation of particles was also observed after second pass FSW due to repeated stirring action of tool [26]. Furthermore, increasing the number of passes refined and uniform distribution of particles were found. Figure 7d reveals that SiC particles size was reduced and

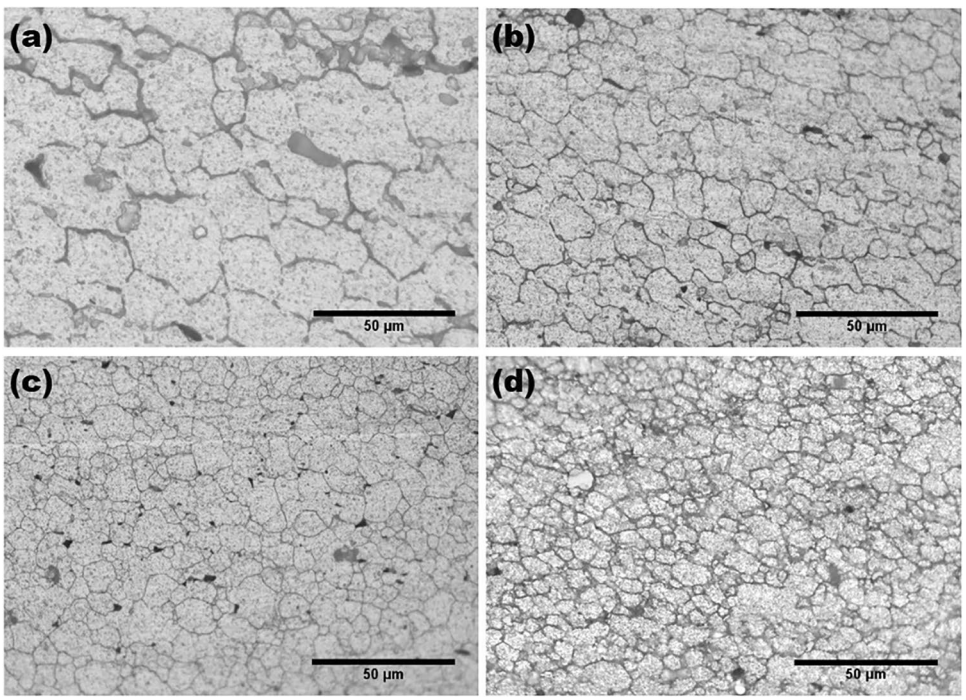

Fig. 6 Optical microscopy image of NZ (**a**) first pass, (**b**) second pass, (**c**) third pass, and (**d**) fourth pass

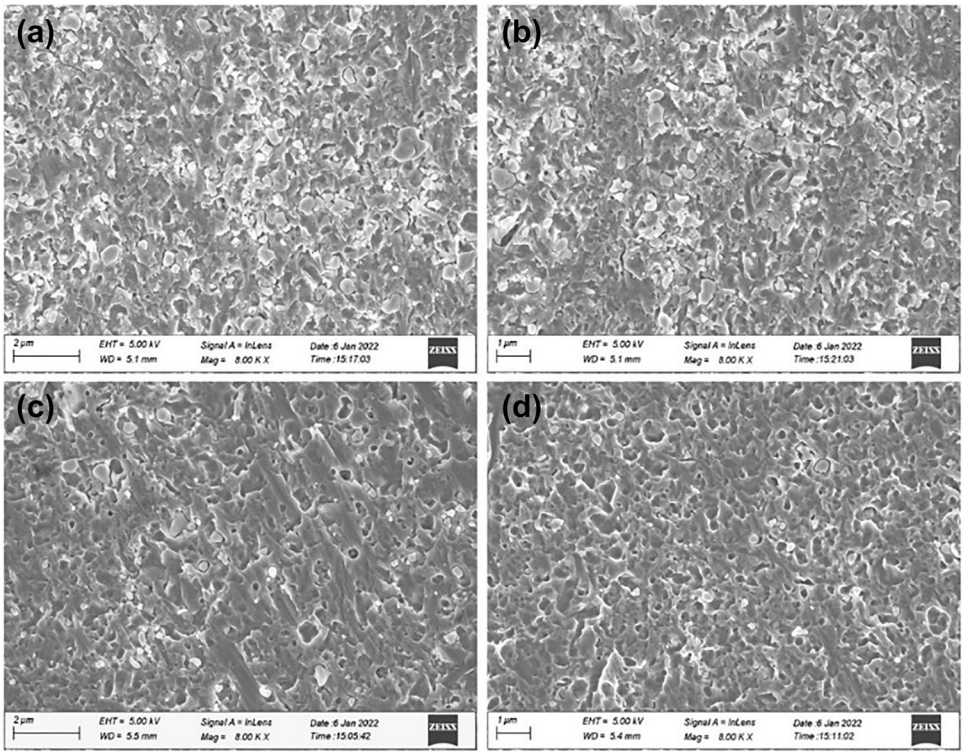

Fig. 7 SEM image of SiC Particles distribution in NZ of (**a**) first pass, (**b**) second pass, (**c**) third pass, and (**d**) fourth pass

uniformly scattered over NZ, in fourth pass FSP compared to the first, second, and third pass FSP. Energy Dispersive Spectroscopy (EDS) analysis of NZ after fourth pass FSP shown in Fig. 8a. The main components of the AA6061 alloy are shown in spectrum 2, while silicon and carbon particles were present as a matrix reinforcing element in spectrum 1 shown in Fig. 8b. As a result of the EDS analysis, it can be said that NZ is composed of SiC particles and AA6061 alloy and silicon mapping also confirms the uniform dispersion of SiC particles in NZ after fourth pass of FSP.

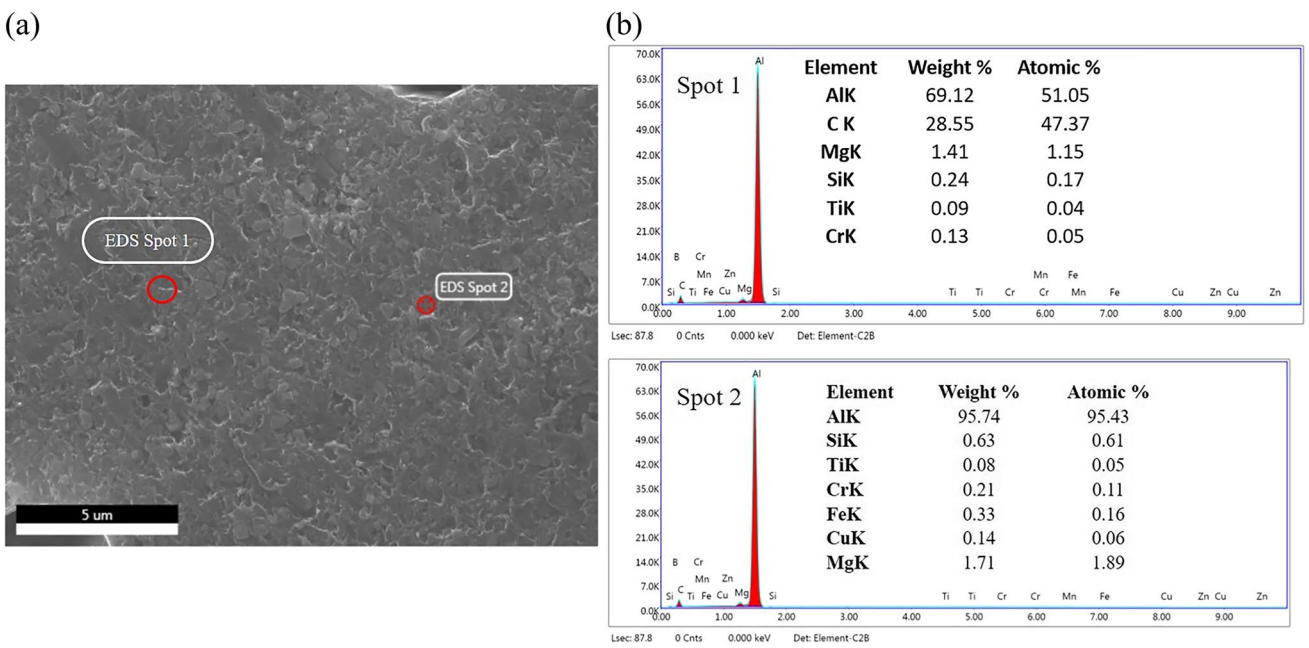

Fig. 8 **(a)** Energy-dispersive spectroscopy analysis, (**b**) Elemental composition analysis

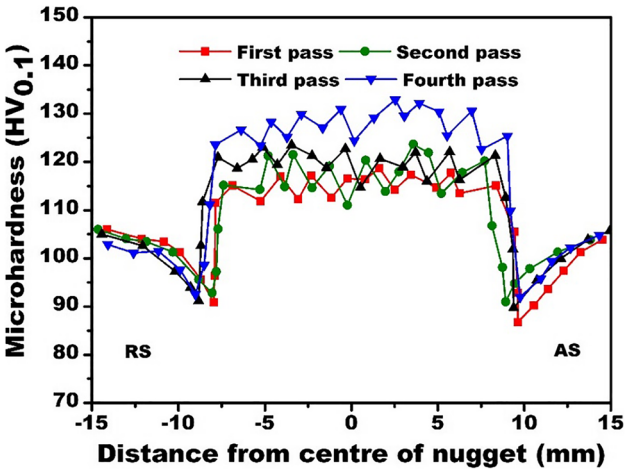

Fig. 9 Microhardness curve of MPFSP of AA6061-T6/SiCp

3.4 Mechanical Properties of MPFSPed AA6061/SiCp

3.4.1 The Effect of Multi-pass FSP AA6061-T6/SiCp on Microhardness

Figure 9 depicts the microhardness value distribution of AA6061-T6/SiC in the different weld region at various FSP passes. The microhardness profile was determined perpendicular to the processing direction in MPFSPed specimen. Observed from the Fig. 9, as the number of passes increases, the hardness value increases. Meanwhile, it can be caused due to the grain fragmentation and refinement of SiC particles [34]. the increase in microhardness value (117.2 HV) during single pass FSP is lower in compared to other FSP pass. However, because of agglomeration and uneven distribution of SiC particles, the microhardness curve in the first pass was inconsistent. Attributable to the recrystallization mechanism and pinning effect of micro-size SiCp, the highly improved microhardness value reported after fourth pass FSP is mostly due to homogenous distribution of SiC particles and finer grain refinement. Azimzadegan et al. [43] & Fulller et al. [44] studied the comparison between the base metal AA6061 and other passes, the fourth pass FSP demonstrated a very fine grain structure. As a result, the influence of grain refinement, high hardness and homogenous distribution reinforcement may be contributed to the enhancement of microhardness value during multi-pass FSP. The effect of multi-pass FSP at constant traverse speed is accompanied by SZ softening. This softening is due to the increased number of passes and greater particle size. The relationship between hardness and grain size has already been correlated using the Hall–Petch equation [45, 46].

$$H_v = H_0 + \frac{K_H}{\sqrt{d}} \quad (1)$$

Where, H_0 is intrinsic hardness of the alloy, K_H is Hall–Petch coefficient, d is the average grain size diameter. According to Eq. (1), particle size is inversely related to hardness, hence smaller grains have a higher hardness value. Because of the lower grain size, the fourth pass has a greater microhardness value (132.3 HV) as compared to first, second and third passes.

3.4.2 The Effect of MFSP AA6061-T6/SiCp on Tensile Strength

Figure 11 shows the UTS, 0.2% yield stress, and % elongation of AA6061-T6/SiC MPFSP. The SiC particles have a favourable impact on both UTS and 0.2% yield stress. The average tensile strength of the AA6061-T6 of base material were 315 MPa observed, and the joint efficiency was calculated as [47].

$$\text{Joint efficiency} = \frac{\text{Tensile Strength of welded joints}}{\text{Tensile strength of base material (AA6061)}} \times 100$$

The efficiency of first, second, third and fourth FSP/SiC pass was found to be 73.33%, 78.41%, 93.96%, and 97.77% respectively, as compared with base material. The stress—strain diagram of the base material and MPFSP of AA6061-T6/SiC is illustrated in Fig. 10. The universal testing was used to study the tensile strength of the MPFSPed specimen of AA6061-T6. Observed from Fig. 11a-b, as the number of passes increased, the UTS and 0.2% yield stress increased from 231 to 308 MPa and 178 MPa to 225 MPa, respectively. The first pass of FSP found to be lower strength of UTS and 0.2% yield stress than BM strength. this may be

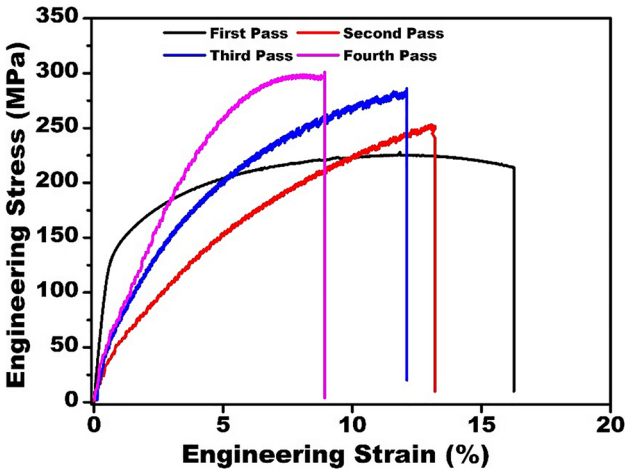

Fig. 10 Engineering stress – strain diagram of MPFSP of AA6061-T6/SiC

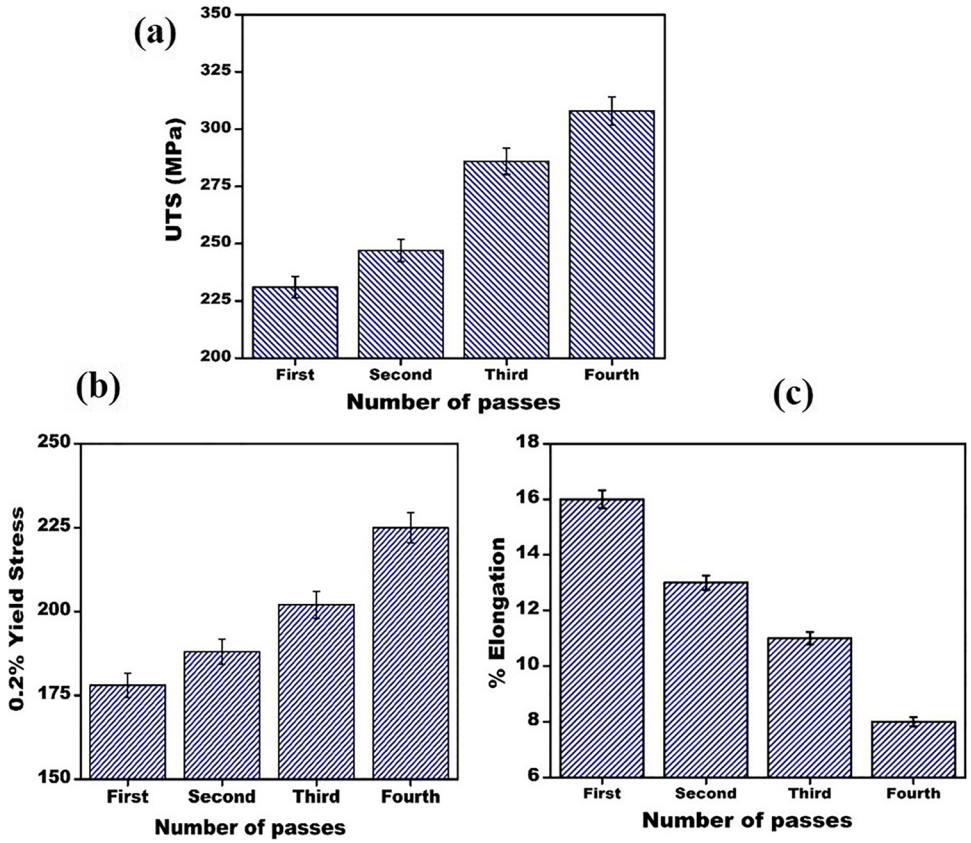

Fig. 11 (**a**) UTS (**b**) 0.2% yield stress and (**c**) % elongation of MPFSP

attributed to SiCp agglomeration at some regions, due to inadequate stirring and uneven SiCp distribution. The interfacial bonding between BM and SiCp decreased, leading in crack propagation and a decrease in UTS and 0.2%. yield stress. Furthermore, it is evident from the Fig. 11a-b that UTS and 0.2% yield stress of the second FSP pass increased 247 MPa and 188 MPa, respectively, although % elongation has decreased (Fig. 11c), due primarily to the proper stirring action.

The homogeneous dispersion of SiCp amplifies the pinning action of SiCp. This increase UTS and 0.2% yield stress in the third and fourth passes FSP, respectively, from 286 to 308 MPa and 202 MPa to 225 MPa. The significant increase in UTS and 0.2% yield stress, but substantial decrease in % elongation, is owing to enhanced fine grain refinement generated by vigorous tool stirring.

Furthermore, increasing the number of passes decreased inter-particle gaping and improved BM and SiCp interfacial compatibility. This feature enhances UTS and 0.2% yield stress. The grain size increases as the distance between inter-particles increases, and the material's strength decreases [48, 49]. The UTS and 0.2% yield stress improved synchronously as the FSP pass increased. The First, second, third, and fourth passes of UTS and 0.2% yield stress was observed as 231 MPa, 247 MPa, 296 MPa, 308 MPa and 178 MPa, 188 MPa, 202 MPa, 225 MPa, respectively.

3.5 Fractography Morphology

SEM was used to investigate the fractured surface in order to see how the microstructure influenced the failure pattern of the processed specimens. The fractographic image of the cracked tensile test specimens MPFSPed of AA6061/SiCp was examined. There are four samples that were tested for each pass of FSP, as shown in Fig. 12.

The combined effect of heat input, grain size, hardness, and particle size must be thoroughly investigated to determine the mode of failure and location for all samples [29]. The tensile fracture outside the NZ reflects well-bonded interactions between the reinforcement particles and the aluminium matrix. Hamdollahzadeh et al. [50] also reported the fracture take place outside the NZ due to good bonding between reinforcement particles and aluminium matrix. At the first pass of FSP, the particles accumulated, which produced large deep dimples and micro-voids (Fig. 13a). This decreased the tensile strength and indicated a fracture of ductile nature. The first pass sample was a raptured interface between the thermo-mechanically affected zone (TMAZ) and heat-affected zone (HAZ) in RS, as illustrated in Fig. 13a. The existence of deep dimples on the tensile fracture indicates a ductile mode of fracture [51].

Furthermore, the aggregation of particles is reduced as the number of passes increases. As a result of the second pass

Fig. 12 Location of fracture surface of AA6061-T6/SiC (**a**) first pass, (**b**) second pass, (**c**) third pass, and (**d**) fourth pass

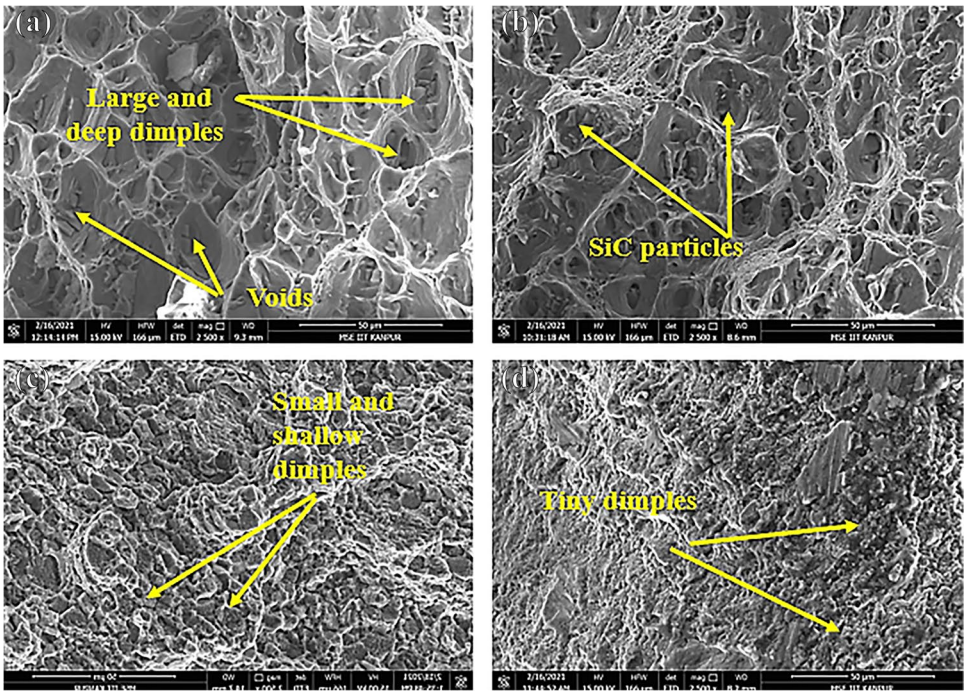

Fig. 13 Fractography of AA6061-T6/SiC (**a**) First Pass (**b**) second pass (**c**) third pass, and (**d**) fourth pass

of FSP, SiC particles scattered unevenly throughout the processed region, as shown in Fig. 13b, and the sample failed on AS of the TMAZ, where hardness was lower. According to [41], the primary cause of the fraction was a raptured interface with cleavage and dimples. While the third pass sample also indicates a ductile mode of failure and raptures in the AS of TMAZ illustrated in Fig. 13c. Barmouz et al. [52] also confirmed the ductile mode of failure by the presence of as small dimples. This is due to the specimen's smaller grain size, which provides more excellent fracture resistance. The fourth pass of the FSP reveals a homogeneous distribution of SiC particles and tiny dimples that increase in tensile strength that transitions to ductility in nature and sample fractured in AS of TMAZ as shown in the Fig. 13d. Husain Mehdi et al. [53] they compared to the one-pass FSP/ZrB2, the fourth pass FSP had fine, homogeneous dimples that were much clearer to see, which are well-known ductile fracture features. The size of the dimples decreases with an increase in passes [54].

4 Conclusion

SiC particles was successfully inserted into multi-pass FSP developed aluminium alloy-based metal matrix composites. Inserting a k-type thermocouple in the AA6061-T6 plate, which is associated with data acquisition to record the temperature distribution during the processing, for investigation of thermal characteristics. The effect of SiCp on temperature

distribution was investigated. The following are some of the findings of this research:

- The incorporation of SiC particles during MPFSP improved significantly UTS, 0.2% yield stress, and microhardness.
- MPFSP implies overlapping one another to achieve uniform SiC particles dispersion, resulting increases the strength.
- The thermal analysis of MPFSP shows that value of peak temperature profile in each pass decreases with increases in number of passes.
- After MPFSP, peak temperature of first pass, second pass, third pass and fourth pass were recorded as 339.67 °C, 330.64 °C, 320.20 °C and 312.81 °C respectively in AS, similarly in RS recorded as 334.03 °C, 322.11 °C, 312.30 °C and 303.72 °C respectively.
- The microhardness value was consistently increasing with MPFSP, observed that first, second, third, and fourth passes of 117.2 HV, 120.6 HV,124.8 HV, and 132.3 HV
- In MPFSP, SiC particles were found to be completely fragmented and dispersed uniformly. With increasing the number of passes, agglomeration of SiC particles decreases. Uniform distribution of particles was observed after the fourth FSP pass.
- After performing MPFSP on AA6061/SiC, the UTS and 0.2% yield stress of the first, second, third, and fourth passes were 231 MPa, 247 MPa, 296 MPa, 308 MPa, and 178 MPa, 188 MPa, 202 MPa, 225 MPa, respectively.

Acknowledgements The first author wishes to thank the Ministry of Human Resource Development of India for giving funding in the form of a fellowship. The authors would like to thank the MSE department, ACMS at IIT Kanpur (specifically Mrs. Samata Samal, Anoop Kumar Raut for microscopic imaging analysis and tensile testing) for their cooperation and smooth testing.

Author Contribution Setu Suman: Conceptualization, Writing—original draft, Investigation, Visualization, Durjyodhan Sethi: Formal analysis, Methodology, resources, Manish Bhargava: review & editing Barnik Saha Roy: review & editing.

Data availability The authors confirm that the data supporting the findings of this study are available within the article.

Declarations

Ethics Approval Not Applicable.

Consent for Publication Consent was obtained from all the authors for the publication of this manuscript.

Consent to Participate Not Applicable.

Conflict of Interest The authors declare that they have no known competing financial interests.

References

1. Pasha MA, Reddy PR, Laxminarayana P, Khan IA (2016) Mechanical behavior of silicon carbide reinforced friction stir welded joint of aluminium alloy 6061. Int J Eng Res 5(05)
2. Zuhailawati H, Anasyida AS (2019) Investigation of the microstructure, mechanical and wear properties of AA6061-T6 friction stir weldments with different particulate reinforcements addition. J Mater Res Technol 8(5):3917–3928
3. Rathee S, Maheshwari S, Siddiquee AN, Srivastava M (2018) A review of recent progress in solid state fabrication of composites and functionally graded systems via friction stir processing. Crit Rev Solid State Mater Sci 43(4):334–366
4. Sethi D, Acharya U, Kumar S, Shekhar S, Roy BS (2022) Effect of tool rotational speed on friction stir welded AA6061-T6 scarf joint configuration. Advanced Composites and Hybrid Materials, pp 1–16
5. Elangovan K, Balasubramanian V, Valliappan M (2008) Effect of tool pin profile and tool rotational speed on mechanical properties of friction stir welded AA6061 aluminium alloy. Mater Manuf Processes 23(3):251–260
6. Thomas WM, Nicholas ED, Needham JC, Murch MG, Templesmith P, Dawes CJ (1991) International Patent Application No. PCT/GB92/02203 and GB Patent Application No. 9125978.8
7. Selvakumar S, Dinaharan I, Palanivel R, Babu BG (2017) Development of stainless steel particulate reinforced AA6082 aluminum matrix composites with enhanced ductility using friction stir processing. Mater Sci Eng, A 685:317–326
8. Dinaharan I, Balakrishnan M, Selvam JDR, Akinlabi ET (2019) Microstructural characterization and tensile behavior of friction stir processed AA6061/Al2Cu cast aluminum matrix composites. J Alloys Compd 781:270–279
9. Dawes CJ (1995) Friction stir joining of aluminium alloys. Bulletin 6
10. Ceschini L, Boromei I, Minak G, Morri A, Tarterini F (2007) Effect of friction stir welding on microstructure, tensile and fatigue properties of the AA7005/10 vol.% Al2O3p composite. Compos Sci Technol 67(3–4):605–615
11. Sharifitabar M, Sarani A, Khorshahian S, Afarani MS (2011) Fabrication of 5052Al/Al2O3 nanoceramic particle reinforced composite via friction stir processing route. Mater Des 32(8–9):4164–4172
12. Sharma A, Sharma VM, Mewar S, Pal SK, Paul J (2018) Friction stir processing of Al6061-SiC-graphite hybrid surface composites. Mater Manuf Processes 33(7):795–804
13. Sharma DK, Patel V, Badheka V, Mehta K, Upadhyay G (2019) Fabrication of hybrid surface composites AA6061/(B4C+ MoS2) via friction stir processing. J Tribol 141(5)
14. Sharma V, Prakash U, Kumar BM (2015) Surface composites by friction stir processing: A review. J Mater Process Technol 224:117–134
15. Khademi AR, Afsari A (2017) Fabrications of surface nanocomposite by friction stir processing to improve mechanical and microstructural properties of low carbon steel. Trans Indian Inst Met 70(5):1193–1198
16. Alavi Nia A, Nourbakhsh SH (2016) Microstructure and mechanical properties of AZ31/SiC and AZ31/CNT composites produced by friction stir processing. Trans Indian Inst Met 69(7):1435–1442

17. Akramifard HR, Shamanian M, Sabbaghian M, Esmailzadeh M (2014) Microstructure and mechanical properties of Cu/SiC metal matrix composite fabricated via friction stir processing. Mater Des 1980–2015(54):838–844
18. Mishra RS, Ma ZY, Charit I (2003) Friction stir processing: a novel technique for fabrication of surface composite. Mater Sci Eng, A 341(1–2):307–310
19. Zahmatkesh B, Enayati MH (2010) A novel approach for development of surface nanocomposite by friction stir processing. Mater Sci Eng, A 527(24–25):6734–6740
20. Shafiei-Zarghani A, Kashani-Bozorg SF, Zarei-Hanzaki A (2009) Microstructures and mechanical properties of Al/Al2O3 surface nano-composite layer produced by friction stir processing. Mater Sci Eng, A 500(1–2):84–91
21. Sahraeinejad S, Izadi H, Haghshenas M, Gerlich AP (2015) Fabrication of metal matrix composites by friction stir processing with different particles and processing parameters. Mater Sci Eng, A 626:505–513
22. Kumar A, Mahapatra MM, Jha PK, Mandal NR, Devuri V (2014) Influence of tool geometries and process variables on friction stir butt welding of Al–4.5% Cu/TiC in situ metal matrix composites. Mater Des 59:406–414
23. Dinaharan I, Murugan N (2012) Effect of friction stir welding on microstructure, mechanical and wear properties of AA6061/ZrB2 in situ cast composites. Mater Sci Eng, A 543:257–266
24. Yuvanarasimman P, Malayalamurthi R (2018) Studies on fractures of friction stir welded Al matrix SiC-B4C reinforced metal composites. SILICON 10(4):1375–1383
25. Mishra RS, Ma ZY (2005) Friction stir welding and processing. Mater Sci Eng R Rep 50(1–2):1–78
26. Jamalian HM, Ramezani H, Ghobadi H, Ansari M, Yari S, Givi MKB (2016) Processing–structure–property correlation in nano-SiC-reinforced friction stir welded aluminum joints. J Manuf Process 21:180–189
27. Rathee S, Maheshwari S, Siddiquee AN (2018) Issues and strategies in composite fabrication via friction stir processing: a review. Mater Manuf Processes 33(3):239–261
28. Srivastava M, Rathee S (2021) A study on the effect of incorporation of SiC particles during friction stir welding of Al 5059 alloy. SILICON 13(7):2209–2219
29. Sethi D, Acharya U, Kumar S, Shekhar S, Roy BS (2021) Effect of reinforcement particles on friction stir welded joints with scarf configuration: an approach to achieve high strength joints. Silicon 1–14
30. Sun YF, Fujii H (2011) The effect of SiC particles on the microstructure and mechanical properties of friction stir welded pure copper joints. Mater Sci Eng, A 528(16–17):5470–5475
31. Dolatkhah A, Golbabaei P, Givi MB, Molaiekiya F (2012) Investigating effects of process parameters on microstructural and mechanical properties of Al5052/SiC metal matrix composite fabricated via friction stir processing. Mater Des 37:458–464
32. Kumar M, Kumar R, Kore SD (2020) Study of temperature distribution and material flow in friction stir welding of AA6061-T6.
33. Rathee S, Maheshwari S, Siddiquee AN, Srivastava M (2019) Investigating the effects of SiC particle sizes on microstructural and mechanical properties of AA5059/SiC surface composites during multi-pass FSP. SILICON 11(2):797–805
34. Mehdi H, Mishra RS (2021) Effect of multi-pass friction stir processing and SiC nanoparticles on microstructure and mechanical properties of AA6082-T6. Adv Ind Manuf Eng 3:100062
35. Jain R, Pal SK, Singh SB (2016) A study on the variation of forces and temperature in a friction stir welding process: a finite element approach. J Manuf Process 23:278–286
36. Kumar AV, Balasrinivasan M, Kumar RV, Balachandar K, Sivakumar C (2020) Temperature distribution study of friction stir welded aluminum alloy 7075–T6 joints reinforced with SiC powders. Materials Today: Proceedings 22:1333–1340
37. Mehdi H, Mishra RS (2020) Influence of friction stir processing on weld temperature distribution and mechanical properties of TIG-welded joint of AA6061 and AA7075. Trans Indian Inst Met 73(7):1773–1788
38. Rathee S, Maheshwari S, Siddiquee AN, Srivastava M (2017) Investigating effects of groove dimensions on microstructure and mechanical properties of AA6063/SiC surface composites produced by friction stir processing. Trans Indian Inst Met 70(3):809–816
39. Kumar N, Gautam G, Gautam RK, Mohan A, Mohan S (2016) Wear, friction and profilometer studies of insitu AA5052/ZrB2 composites. Tribol Int 97:313–326
40. Zapata-Solvas E, Jayaseelan DD, Lin HT, Brown P, Lee WE (2013) Mechanical properties of ZrB2-and HfB2-based ultra-high temperature ceramics fabricated by spark plasma sintering. J Eur Ceram Soc 33(7):1373–1386
41. Hashmi AW, Mehdi H, Mishra RS, Mohapatra P, Kant N, Kumar R (2022) Mechanical properties and microstructure evolution of AA6082/sic nanocomposite processed by multi-pass FSP. Trans Indian Inst Met 1–14
42. Chang CI, Lee CJ, Huang JC (2004) Relationship between grain size and Zener-Holloman parameter during friction stir processing in AZ31 Mg alloys. Scripta Mater 51(6):509–514
43. Azimzadegan T, Serajzadeh S (2010) An investigation into microstructures and mechanical properties of AA7075-T6 during friction stir welding at relatively high rotational speeds. J Mater Eng Perform 19(9):1256–1263
44. Fuller CB, Mahoney MW, Calabrese M, Micona L (2010) Evolution of microstructure and mechanical properties in naturally aged 7050 and 7075 Al friction stir welds. Mater Sci Eng, A 527(9):2233–2240
45. Sethi D, Acharya U, Shekhar S, Roy BS (2022) Applicability of unique scarf joint configuration in friction stir welding of AA6061-T6: analysis of torque, force, microstructure and mechanical properties. Defence Technology 18(4):567–582
46. Kumar S, Acharya U, Sethi D, Medhi T, Roy BS, Saha SC (2020) Effect of traverse speed on microstructure and mechanical properties of friction-stir-welded third-generation Al–Li alloy. J Braz Soc Mech Sci Eng 42(8):1–13
47. Pandey C, Mahapatra MM, Kumar P, Thakre JG, Saini N (2019) Role of evolving microstructure on the mechanical behaviour of P92 steel welded joint in as-welded and post weld heat treated state. J Mater Process Technol 263:241–255
48. Ceschini L, Boromei I, Minak G, Morri A, Tarterini F (2007) Microstructure, tensile and fatigue properties of AA6061/20 vol.% Al2O3p friction stir welded joints. Compos A: Appl Sci Manuf 38(4):1200–1210
49. Marzoli LM, Strombeck AV, Dos Santos JF, Gambaro C, Volpone LM (2006) Friction stir welding of an AA6061/Al2O3/20p reinforced alloy. Compos Sci Technol 66(2):363–371
50. Hamdollahzadeh A, Bahrami M, Nikoo MF, Yusefi A, Givi MB, Parvin N (2015) Microstructure evolutions and mechanical properties of nano-SiC-fortified AA7075 friction stir weldment: The role of second pass processing. J Manuf Process 20:367–373
51. Banik A, Roy BS, Barma JD, Saha SC (2018) An experimental investigation of torque and force generation for varying tool tilt angles and their effects on microstructure and mechanical properties: Friction stir welding of AA 6061–T6. J Manuf Process 31:395–404

52. Barmouz M, Asadi P, Givi MB, Taherishargh M (2011) Investigation of mechanical properties of Cu/SiC composite fabricated by FSP: Effect of SiC particles' size and volume fraction. Mater Sci Eng, A 528(3):1740–1749
53. Mehdi H, Mishra RS (2022) Modification of microstructure and mechanical properties of AA6082/ZrB2 processed by multipass friction stir processing. J Mater Eng Perform 1–11
54. Maeda M, Liu H, Fujii H, Shibayanagi T (2005) Temperature field in the vicinity of FSW-tool during friction stir welding of aluminium alloys. Weld World 49(3):69–75

Publisher's Note Springer Nature remains neutral with regard to jurisdictional claims in published maps and institutional affiliations.

Springer Nature or its licensor holds exclusive rights to this article under a publishing agreement with the author(s) or other rightsholder(s); author self-archiving of the accepted manuscript version of this article is solely governed by the terms of such publishing agreement and applicable law.